

CITO Implementation paper 16:

A novel method for dendrochronology of large historical wooden objects using line trajectory X-ray tomography

Martijn Combé (s2599406), Daniel Zee (s2063131)

Abstract—This paper presents new methods for evaluating and testing line trajectory X-ray tomography on realistic 3D phantoms of wooden objects. Using a X-ray line trajectory and the SIRT algorithm, non evasive reconstructions can be made for wooden objects. The proposed methods are based on a new quantified metric called Weighted Radial Correlation Over All Angles (WRCOAA) and weighted radial correlation over longest angles (WRCOLA). The metric is used to compare reconstructions at different depths, tree-ring tilts, and projection cone angles, as well as testing of ideal depth, cone angle and tree tilt angle combinations. The metrics provide a better understanding of reconstruction quality for reconstructions in the field of dendrochronology, compared to SSIM. It was found that wooden objects with larger tree-ring tilts can be reconstructed using larger cone beam angles.

I. INTRODUCTION

IN the field of dendrochronology, or tree-ring science, it is often important to use non-invasive procedures for visualizing the tree-ring structures in a wooden object. Bossema [1] introduced such a method using a standard X-ray source and a detector. The wooden object is moved sideways in a line trajectory, with the transverse section perpendicular to the source-detector axis. Iterative reconstruction algorithms can then be used to reconstruct the tree rings within the wooden object. In order to reconstruct this research, we created realistic phantoms for simulating wooden objects with adjustable tree-ring tilts in both the height and width axis. Using these phantoms, we performed the proposed method using the ASTRA Toolbox [2] for defining the linear projection trajectory, creating forward projections, and reconstructing the tree ring patterns in the transverse section using SIRT.

We investigated what effect different parameter choices have on the quality of the reconstructions and extended the limits of the method, by answering the following research question:

RQ 1: How can dendrochronology of wooden objects using line trajectory X-ray tomography be improved?

To do this, better statistical methods were needed in order to compare the quality of different reconstructions, which leads

to the first sub-question:

RQ 1.1: How can the practical quality of tree-ring reconstructions be quantified and compared?

The slice depth of the wooden block that is observed determines the quality of the reconstruction. While the authors of the original paper picked this depth based on observations, we attempted to find a more general optimal reconstruction depth more analytically, by answering the following sub-question:

RQ 1.2: At which relative depth along the phantom are slice reconstructions of the highest practical quality?

The final parameter that can be adjusted is the angle of the cone beam used in the X-ray setup. The paper suggests that the maximum horizontal tree-ring tilt angle α_h which can be accurately reconstructed is constrained by the cone angle β . We investigated whether this suggestion is true, and whether increasing β will lead to higher quality reconstructions for a wider range of tree-ring tilts. In order to investigate this relation, the following sub-question was answered:

RQ 1.3: How does the interplay between the tree-ring angles in both axis and the projection cone angle impact the practical quality of the tree-ring reconstructions?

In order to answer these questions, extensive testing was done using our phantom generator, and newly implemented measurement collection.

This section provides an introduction to the problem; section II will describe the related work of Bossema and will provide extra background regarding the field of dendrochronology; section III will explain the algorithm that was used and how we implemented extra quality measurements; section IV will provide explanations of how the phantom data was generated, and will explain the experiments that were done in order to answer the research questions; section V will explain the results that were gathered from the experiments, and in

section VI we will discuss them and provide future work; In section VII we will conclude by providing a summary each section and highlight the main findings of this paper.

June 13, 2025

II. RELATED WORK

In this section, some extra background regarding the original paper and dendrochronology is provided. This will give an idea of the problem at hand and provide explanation of terms used in future sections.

The research by F. Bossema[1] goes in depth on the importance of using non-evasive methods when scanning wooden objects. The research specifically investigates X-ray methods for scanning large wooden historical objects, like the famous Dutch book chest of Hugo de Groot that was used for testing their experiments in real-world situations [3]. It is especially important not to damage the object, when they are of historical importance. Counting tree rings is however something that can help determining the age of an object. This is done in the field of dendrochronology, or tree-ring-science. Since the tree rings in the object have different chemical compositions, they can be counted into a chronological series, and mapped into a specific sequence of calendar years in time [4], or climate conditions at time of growth [5]. When longer sequences can be identified, these predictions become more accurate. Traditionally however, this could only be done by taking a physical slice of the object and counting the rings, which damages the object. Instead, computed tomography (CT) can be used which provides useful 3D information. This however requires full rotation around the objects, which is not useful for very large objects. Therefore, the paper presented a line-trajectory with an X-ray source. This method works, because the difference in ring-density provides contrast, as a result of the amount of radiation that passes trough a ring. This however blurs part of the rings, as the beams become weaker as they pass trough the object. Using a cone beam and a line trajectory for the source object, it is possible to gather enough information to create a reasonable reconstruction where only the edges are less sharp. Due to a smearing effect, the ideal depth (slice) to reconstruct was found not to be at the exact front of the object, but was chosen around 25 percent, based on the observations of the author. Another idea that was investigated is the tilt of the tree rings within the object. This is because the rings in the object are not necessarily aligned with the source-detector axis. Therefore a tree-ring tilt α is defined, where a tilt of $\alpha = 0^\circ$ is the case where the rings are parallel with the source-detector axis. It was found that when using a cone angle β of 9° , angles α that are smaller than β result in accurate reconstructions of the phantom slices. When this α is exceeded, the reconstructed image becomes too blurred. It is however noted that cone beam angle β is not a hard limit for the tree-ring tilt, which is something that will be investigated in this paper. When describing the directions in a wooden object, the field dendrochronology uses the terms transverse, radial and tangential. These relate to the direction of the tree-rings, and are illustrated in figure 1.

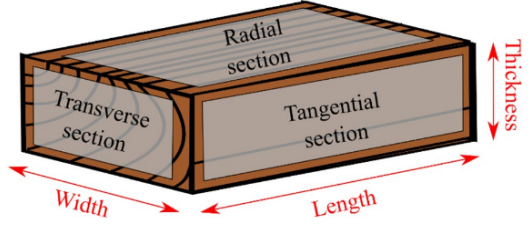


Fig. 1. Illustration of terms used in the field of dendrochronology when describing directions of a wooden object [1].

III. METHODS

This section will describe the implemented methods for generating phantoms, creating reconstructions using SIRT, and the implemented methods for measuring the difference in quality between reconstructions.

A. Phantom Generation

In order to test the proposed methods and perform our experiments, representative phantoms of wooden objects were needed. These phantoms must be simulated 3D objects representing blocks of wood with internal tree-rings structures. While tree rings move linearly through an object, they are rarely situated in parallel to the radial and tangential sections in real life objects. The phantoms should therefore also be able to simulate this tree-ring tilt, as it can influence the robustness of the proposed method. The creation of the testing data will be further discussed in section IV.

B. ASTRA Toolbox

As we are performing the CT reconstructions on simulated objects, both the forward projection and reconstruction operations are performed using software. For this purpose, the ASTRA Toolbox was used. The ASTRA Toolbox provides a highly efficient and highly flexible open source set of tools for tomographic projection and reconstruction [2]. This flexibly allowed us to specify the required linear projection trajectory, using the included vector-based projection geometry specification.

The ASTRA Toolbox requires a volume geometry and a projection geometry to be defined. The phantoms used have a width of 800 and a height of 600 pixels in the transverse section, paired with a depth of 2000 pixels. As we are only interested in reconstructing the transverse section at a good enough point along the depth of the object, we do not need our volume geometry to have the full resolution in the depth axis. The decision was therefore made to use anisotropic voxels in the volume geometry, where only 100 voxels are used to span the 2000 pixels in the depth axis.

For the projection geometry, we defined the horizontal linear trajectory using vector notations for each projection. Figure 2 shows how the source and the detector move along the transverse section of the phantom, starting and ending at the final positions where the phantom is captured by the projection cone. The vector representations of these positions

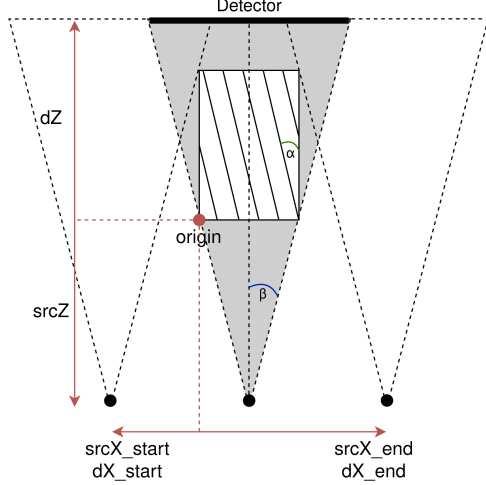


Fig. 2. The projection geometry is defined by a set of vectors, specifying the position of the source and the detector in the volume geometry coordinate system at each projection.

in the volume geometry are automatically calculated given the dimensions of the phantom, the desired cone angle β , and the number of projections.

C. SIRT reconstruction

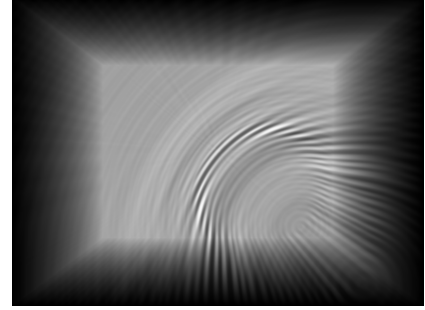
We create sinograms by performing the forward projection and reconstruct our phantom using the built-in GPU accelerated SIRT [7] algorithm provided by ASTRA Toolbox. SIRT is an iterative algebraic reconstruction technique, suitable for asymmetrical projection trajectories.

Figure 3 shows an example reconstruction from a sinogram, using $\beta = 9^\circ$, and $\alpha = 0^\circ$, which were the parameters of the original paper[1]. After reconstruction, we have a reconstruction of the transverse section along 100 evenly spaced steps in the depth of the phantom.

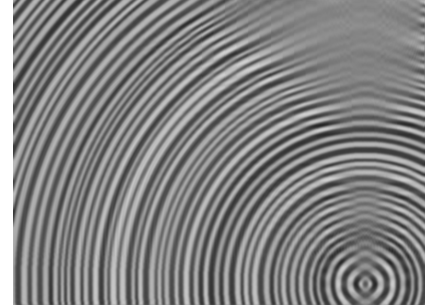
D. Quantified Reconstruction Measurements

After reconstruction, we need measures to determine the quality of transverse slices compared to the phantom. The first measure we used is the structural similarity index measure (SSIM) [6]. SSIM is a perceptual metric that quantifies the visual similarity between two images by comparing their luminance, contrast, and structural information.

For the remaining measures, we developed a domain specific approach, which takes into account the practical usefulness of a reconstruction in the field of dendrochronology. The priority here lies in the ability to accurately count the width between the tree rings, starting from the pith (the center ring) moving towards the edges. The similarity between tree ring width series is often expressed using the Pearson product moment correlation coefficient (PMCC) between the series [8]. To measure the accuracy of the reconstructed tree rings, we therefore extract the radial profile signals starting at the pith and ending at the edge of the image, for all 360 degrees around the pith. We then calculate the PMCC score for all angles, by comparing them to the profiles at the same angles,



(a) The resulting forward projection in the center of the projection trajectory.



(b) SIRT reconstruction for projections, showing the slice perpendicular to the source-detector axis at 25% of the depth of the simulated object

Fig. 3. Example reconstruction from a sinogram. (a) shows the projection in the center of the projection trajectory, (b) shows the SIRT reconstruction for the projection. The sinogram was made using $\beta = 9^\circ$, and a phantom was used with $\alpha = 0^\circ$.

in the phantom. Finally, the PMCC scores over all angles are combined into one score by taking the average weighted by the number of tree rings in the angles, called the Weighted Radial Correlation Over All Angles (WRCOAA).

The final quality measure used is a more constrained version of WRCOAA, where we only take the weighted average over the PMCC scores of angles around the pith which have a ring count above the 80th percentile. This can help us filter out the negative contribution of poorly reconstructed angles with a lower number of rings, as these angles can be viewed as redundant when we have high quality reconstructions over longer angles. We therefore refer to this measure as the Weighted Radial Correlation Over Longest Angles (WRCOLA). Figure 13 of Appendix B shows detailed explanation figures of the construction of the measures.

IV. EXPERIMENTS

In this section we will explain the experiments that were done to answer the research questions, and how realistic phantoms were generated.

A. Phantom generation

In order to conduct experiments to test the method, realistic phantoms are needed that represent 3D wooden blocks. A function was written to generate 2D images, and transforming them into 3D object. Three dimensions must be specified at creation: width, height and depth. Using the width and height,

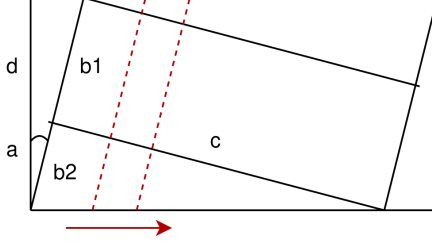


Fig. 4. To generate a phantom with a tree-ring tilt (a) in the height axis, we calculate the height of the wooden object it is cut from (d), using the height (b_1) and depth (c) of our desired phantom. The tree rings are then created for height d , and then vertically resized to length $b_1 + b_2$, to accommodate the angle. A moving window of size b_1 is then linearly moved down the resized tree rings to generate the 3D phantom of depth c . The same method holds for the tree-ring tilt in the width axis.

a 2D grayscale image is created of the transverse tree-rings. The location of the pith is either chosen at random, or placed in the center of the section. The width and grayscale values for each ring are randomly chosen within bounds specified by the user. If no tilt is specified, the final 3D phantom is then created by repeating this transverse section equal to the depth. A tilt can be given for the tree rings in both the height and width axis. When a tilt is given, the width and height of the 2D transverse image are first recalculated using the method described in figure 4. This allows us to accommodate "cutting" our woodling block from the larger wooden block, resulting in the wanted tree-ring tilt. Finally, a Gaussian filter can be applied to blur the transitions between the tree rings.

A function was then written for visualizing the generated 3D phantoms. This viewer function takes the phantom as input and displays an interactive slider to scroll through slices of the 3D grayscale array along different axes. Examples of these generated phantoms can be seen in Appendix A. Figure 10 shows a generated example for a phantom without an angle in both axis, Figures 11 and 12 show generated examples with α of 20 degrees in the height and width axis respectively.

To perform our experiments, two sets of phantoms were generated. The decision was made to place the pith of the phantoms in the center of the transverse section for all experiments, as this allows us to compare results between tree-ring tilt configurations. All phantoms used have a width of 800 and a height of 600 pixels in the transverse section, paired with a depth of 2000 pixels, and are generated with a Gaussian blur with a standard deviation of 2. The first set of phantoms were generated using horizontal tree-ring tilt angles α_h of 0, 6, 8, 10 and 12 degrees, while keeping the vertical tree-ring tilt α_v at 0° . The second phantom set does the inverse, using the same range of values for α_v , while keeping α_h at 0° .

B. Experimental Setup

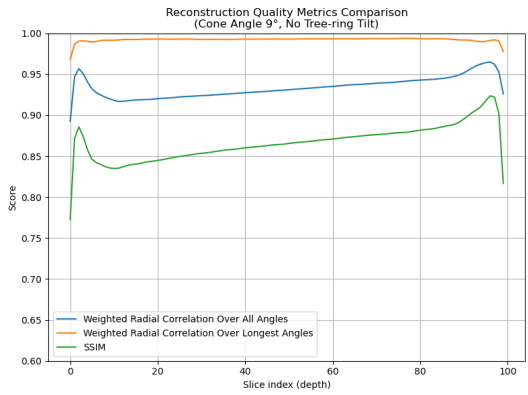
For reconstruction of the phantoms, both sets where reconstructed using projections cone angles $\beta = 9^\circ$, and $\beta = 15^\circ$. Anisotropic sampling was used in the depth of the phantoms with a sampling interval of 20, resulting in 100 evenly spaced transverse sections in the reconstruction. A horizontal linear projection trajectory was used with a total of 101 evenly spaced projections. Reconstructions were made

using the SIRT algorithm with 50 iterations. For our first experiment, we measure the reconstruction quality of all 100 slices from the phantom with $\alpha_h = \alpha_v = 0$, for both cone angles β . The reconstruction quality was expressed using all three previously described quality measures: SSIM, WRCOAA and WRCOLA. This allows us not only to determine the ideal reconstruction depths, but also allows us to compare the used quality measures. For our second experiment, we compare the reconstruction quality of all 100 slices between the phantom set with differing horizontal tree-ring tilt angles α_h . For this phantom set, both the WRCOAA and WRCOLA scores were compared against each other, allowing us to separately judge the changes in reconstruction quality when only considering the longer radial angles from the pith.

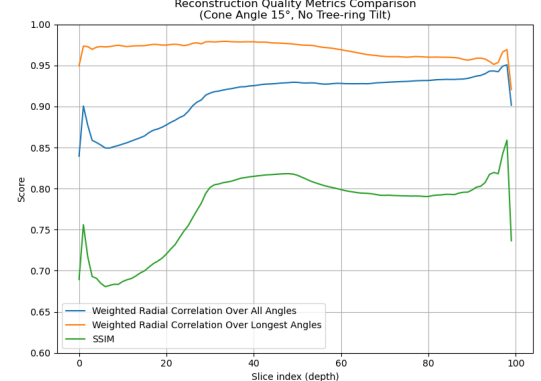
For our final experiment, the same process was performed on the phantom set with differing vertical tree-ring tilt angles α_v .

V. RESULTS

In this section we compare our constructed quality metrics to SSIM, and present the results of using the metric to compare reconstructions at different depths, tree-ring tilts and cone angles.



(a) Projection cone angle of $\beta = 9^\circ$

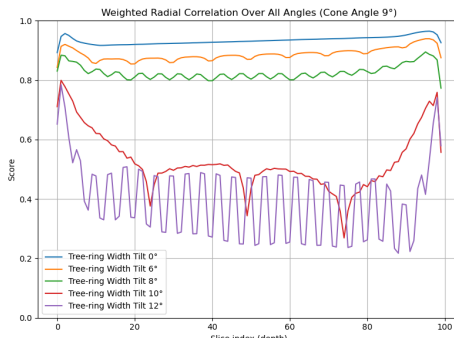


(b) Projection cone angle of $\beta = 15^\circ$

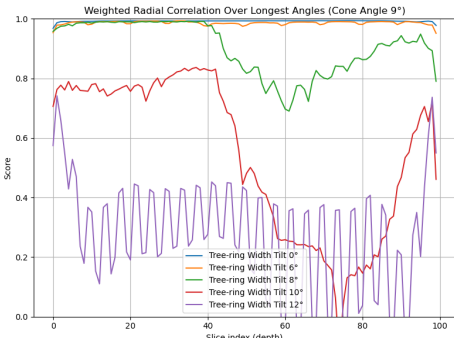
Fig. 5. Comparison of different measurement methods (WRCOAA, WRCOLA and SSIM). (a) shows the scores for a cone angle of $\beta = 9^\circ$, over the slice depth. (b) shows the scores for a cone angle of $\beta = 15^\circ$, over the slice depth. No tree-ring tilt is used. The domain specific approach of WRCOAA and WRCOLA provides a better insight for the ability to count tree rings, compared to SSIM.

A. Slice Reconstructions Quality Measures

Figure 5 shows a comparison between the quality measures on the phantoms without tree-ring tilts for both cone angles. The WRCOAA and SSIM scores appear to be highly correlated, which confirms that our WRCOAA score gives an accurate generalization of the reconstruction quality over the entire image. For both cone angles, the WRCOAA appears to be worst in the first and last slices, which is in line with the findings in the original paper stating that the smearing effect was found to be the worst at the exact front of the object. The WRCOAA scores then decrease in the early stages and climb back up towards the end of the phantoms. An interesting observation however is that the WRCOLA scores do not appear to follow this trend, staying very high all the way for a cone angle of 9 degrees and decreasing towards the end at 15 degrees. As this score only takes into account the radial angles with the highest number of tree rings, we can therefore conclude that the decrease in quality in the early slices is mainly due to redundant angles with lower number of tree ring. This effect can be clearly seen in figure 13 in Appendix B, showing the individual radial correlations of all angles, together with markings for the longest angles, for slice index 9 in the phantom. Furthermore, we can observe that for all metrics, the quality scores for a cone angle of 9 degrees are on average higher than for 15 degrees.



(a) WRCOAA score over depth slices.

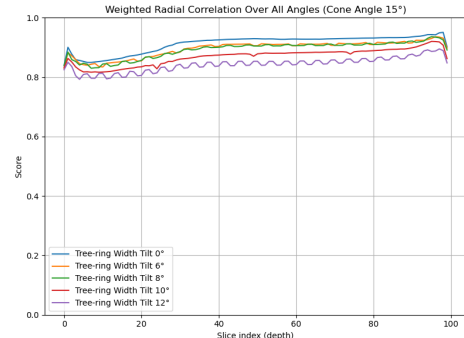


(b) WRCOLA score over depth slices.

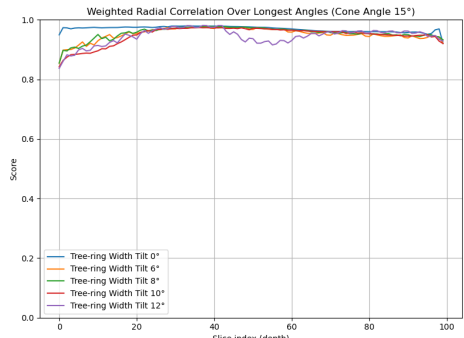
Fig. 6. Scores for different horizontal tree-ring tilt angles, using $\beta = 9^\circ$. (a) shows the WRCOAA score over depth slices, (b) shows the WRCOLA score over depth slices. For larger tree-ring tilts, results are very unstable. Ideal depth seems to be at the front or end of the block. Works reasonably well for smaller tree-ring tilts.

B. Horizontal Tree-Ring Tilt

Figure 6 shows the WRCOAA and WRCOLA scores when gradually increasing the horizontal tree-ring tilts α_h at cone angle of 9 degrees. From the WRCOAA scores, we see a gradual decline in reconstruction quality up to $\alpha_h = 8$. Further increasing α_h above the cone angle leads to a rapid decrease in quality. The WRCOLA scores paint a different picture, showing near perfect reconstructing of the longest angles for all slices at $\alpha_h = 6$, and a collapse in quality around slice 40 for $\alpha_h = 8$. Values higher again show much lower reconstruction quality, even at the earlier slices. To explain these observations, we have to look at Figure 14 in Appendix C, showing the reconstructions at slice 50 at each phantom. We observe that as α_h increases, the burry area in the reconstructions extends more to the right side of the pith. This is the side of the phantom that our method is not able to accurate reconstruct due to it being "behind" the tree-ring tilt. As α_h exceeds the cone angle, we additionally see blurriness appearing on the left side, eventually making the reconstructions unusable. The collapse in the WRCOLA scores can be explained by the fact that due to the tree-ring tilt, the pith is moving from right to left throughout the slices, affecting the angles with the longest tree-ring series. Therefore, as the pith reaches the left half of the image, the longest angles are aimed at the right side of the image, which has a lower reconstruction quality



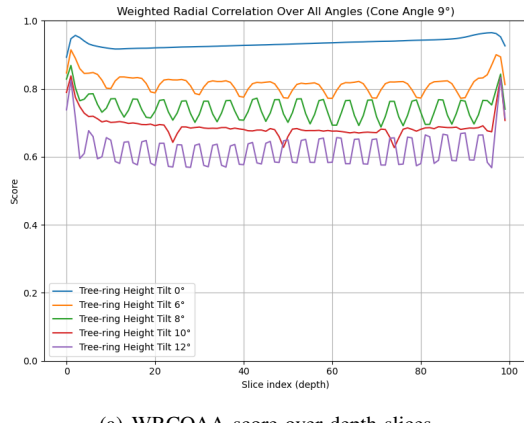
(a) WRCOAA score over depth slices.



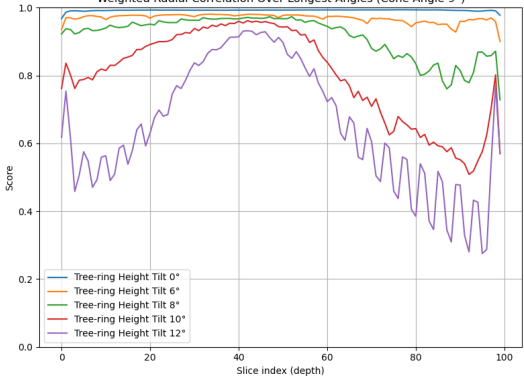
(b) WRCOLA score over depth slices.

Fig. 7. Scores for different horizontal tree-ring tilt angles, using $\beta = 15^\circ$. (a) shows the WRCOAA score over depth slices, (b) shows the WRCOLA score over depth slices. Increasing the cone angle leads to more stable results, especially for larger angles compared to the smaller cone size. Smaller tree-ring tilts do not benefit from larger cone angles.

Figure 7 shows the results for using a bigger cone angle of $\beta = 15^\circ$. Interestingly, it shows that a larger cone angle results in a much more stable reconstruction across different depths for each of the tree-ring tilts. This suggests that there is indeed a relation between the maximum angle of the tree-rings and the cone angle. It is however again important to note that though they are more stable, the overall quality for the smaller tree ring tilts has decreased, indicating a diminishing return in increasing the cone angle. Looking at WRCOLA scores, it can be seen that for each configuration this also leads to higher correlation values. An interesting observation is however that the scores are lower for the first 40 slices when introducing a horizontal tree-ring tilt. This can be explained by inspecting the radial correlations in Figure 13 b. Here we see a decrease in correlation values in the horizontal angles, which were not present at $\beta = 9^\circ$. These angles are not present in the longest angles when the pith is centered, but they are when we pith starts of more to the left, as is the case with the horizontal tree-ring tilts. Figure 15 in Appendix C shows the reconstructions at slice 50 for $\beta = 15^\circ$. We can clearly see that the increased cone angle results in a slower spreading of the blurry regions in the reconstructed images.

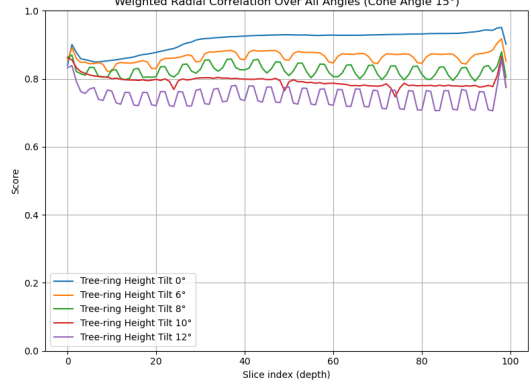


(a) WRCOAA score over depth slices.

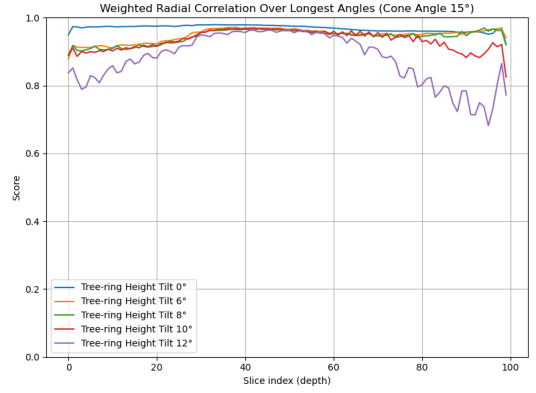


(b) WRCOLA score over depth slices.

Fig. 8. Scores for different vertical tree-ring tilt angles, using $\beta = 9^\circ$. (a) shows the WRCOAA score over depth slices, (b) shows the WRCOLA score over depth slices. A vertical tilt results in more stable scores for larger tilts, and reconstruction depth is of more importance.



(a) WRCOAA score over depth slices



(b) WRCOLA score over depth slices

Fig. 9. Scores for different vertical tree-ring tilt angles, using $\beta = 15^\circ$. (a) shows the WRCOAA score over depth slices, (b) shows the WRCOLA score over depth slices. A larger cone angle results in more stable scores, especially for larger tilts.

C. Vertical Tree-Ring Tilt

When using phantoms with vertical tree-ring tilts instead of horizontal tree-ring tilts, obvious differences can be seen. Figure 8 shows that we no longer observe a drastic collapse in WRCOAA scores after exceeding the cone angle, but instead see a linear decrease in scores throughout the configurations. The Scores for tree-ring tilts below the cone angle are however lower than for their respective horizontal counterparts. The WRCOLA scores show for all angles α_v that the optimal reconstructions of the longest radial angles lie around slice 45. Increasing the cone angle to 15 degrees again appears to improve the overall reconstruction quality. Figure 9 shows that both the WRCOAA and WRCOLA scores have increased, while keeping the same trends seen for $\beta = 9^\circ$. Figures 16 and 17 in appendix D show the reconstructions at slice 50 at each phantom for both cone angles. We see blurry regions in both vertical directions from the pith, with the south blurry region being wider. Increasing α_v leads to an approximately linear spread of the blurry areas, and this spread appears to slow down when increasing the cone angle. It therefore makes sense that we see the highest WRCOLA scores around slice 45, as at that point the pith is a bit south of the center, compensation for the increased blurriness there.

VI. DISCUSSION

As the original paper suggests, finding the right depth slice is key to obtaining the ideal reconstruction quality. However, instead of the depth of 25 percent that was used by the authors based on observations, our results show that this depth heavily depends on multiple conditions, especially the cone beam angle and the tree-ring tilt in both axis. For smaller tree-ring tilts, as compared to the cone angle, this depth appears to be trivial, as decent reconstructions were made at each depth. The ideal depth mostly depends on the location of the pith, as its location in the object determines the relative contribution of the region in the slice which lies "behind" the pith in the reconstruction, for which we can not gather sufficient data during the CT scans. It was therefore also found that wooden objects with a higher tree-ring tilt require a larger cone beam angle in order to achieve high quality reconstructions. This increase in cone angle however has a negative effect on the baseline reconstruction quality, indicating that increasing the cone angle does have diminishing returns. Another interesting observation is that the threshold for the horizontal tree-ring tilt for a given cone angle does not appear to exist for vertical tree-ring tilt, as the reconstruction quality there keeps linearly decreasing for tree-ring tilts which exceed the cone angle. To answer the question whether dendrochronology of wooden objects using line trajectory X-rays can be improved, a comparison must be made between the efforts of the original paper and our results. It was found that larger tree-ring tilts can be used compared to the tilts in the original paper while maintaining decent reconstruction quality, but only when increasing the cone angle. We were also able to extend the possibility of the method by introducing phantoms with vertical tree-ring tilts. The objective of dendrochronology is to count the number of rings in the object, which is definitely possible for the cases in which new configurations were used, as can be seen in appendix C and D. It is however hard to determine an ideal reconstruction depth, as it heavily relies on the tree-ring tilt, cone angle, direction of the trajectory and pith location. Our suspicion is however that this point is often just before the pith crosses the middle of the frame, which was in our case at slice 40 to 45. It should also be noted that this is most likely the result of how the WRCOLA handles the longest angles, which we assume are of most practical use in dendrochronology research.

Though the implemented metrics provide a good framework for comparing reconstructions of the same phantom, they heavily rely on the location of the pith, and the orientation of the object. This is not a big issue when the tree ring tilt is minimal, but as it increases, the location of the pith more heavily influences the region in the transverse sections which can not be reconstructed accurately. When using this method in practice, the tree-ring angles inside of an object are not always known beforehand, so the choice of cone angle and object orientation then needs to be made by trial and error, which could be costly and time consuming. Our methods do however provide a lot of possibilities for testing different types of wooden blocks, mainly due to the extensive possibilities of our phantom generator.

In the future, the results from this paper might be tested in the real world, as it might well be that the parameters picked in the original paper were based on real world reconstructions. Different wood types that vary in density might also change results. An effort could be made to extend the horizontal trajectory to also include a vertical linear trajectory, increasing the linear system of equations to be solved by SIRT, which could theoretically increase the reconstruction quality in the vertical axis. Also, our results show that the pith of the object influence the results significantly, so it could be interesting to see what effect different pith locations would have.

VII. CONCLUSION

This paper introduced new methods for evaluating and testing line trajectory X-ray tomography on realistic 3D phantoms of wooden objects. Counting the rings of a wooden object, as is done in the field of dendrochronology can tell much about the age, origin and environment of wood used for historical objects. However, doing so often requires damaging the object. Bossema [1] introduced a method for scanning these objects with a single line trajectory X-ray. Our implementation extends this work, by adding quantified measurements for comparing reconstructions of the transverse sections of wooden objects along their depth, as well as testing for ideal reconstruction depth, cone angle and tree-ring tilt angle combinations. Besides this, our 3D phantoms provide the possibility to generate tree-ring tilts in both the horizontal and the vertical axis of the object, further extending the testing possibilities. Using a new quantified metric called Weighted Radial Correlation Over All Angles (WRCOAA), and Weighted Radial Correlation Over Longest Angles (WRCOLA) it was found that the maximum tree-ring tilt is indeed constrained by the used cone angle of the source during the forward projection process. The metrics provided a better understanding of reconstruction quality for reconstructions in the field of dendrochronology compared to conventional SSIM. Using larger cone angles and scanning objects where the tree-ring tilt is in the vertical direction, wooden objects with larger tree-ring tilts can be scanned and reconstructed. Reconstructions however heavily relied on the location of the pith (core) of the object, as reconstruction behind the pith are difficult when there is a tree-ring angle. In the future, this method could be tested on real-world wooden objects, the influence of the pith location could be further investigated.

APPENDIX A

EXAMPLES OF PHANTOM GENERATION

This section includes images that were the result of the phantom generation process. They were produced using python and can be viewed in the transverse, radial and tangential section. Using a slider, one can move through different slices of the 3D phantom. Figure 10 includes and example of a wooden phantom without an angle in the tree rings, and Figure 11 and 12 show examples of phantoms with a ring-tree angle of 20 degrees in the height and width axis respectively.

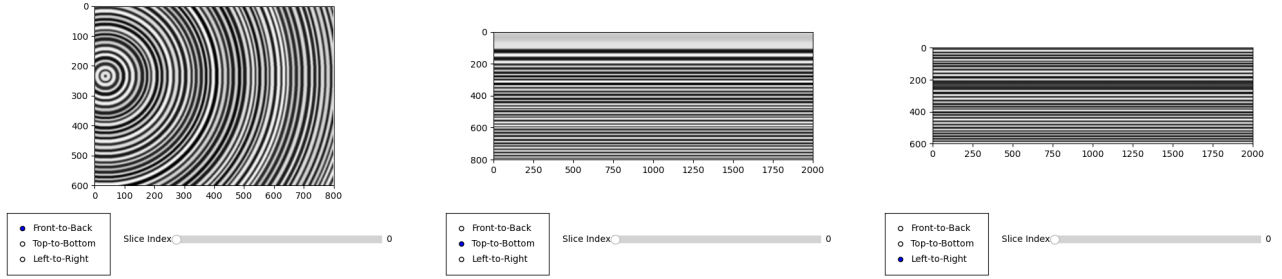


Fig. 10. Phantom for a wooden block of which the rings have no angle.

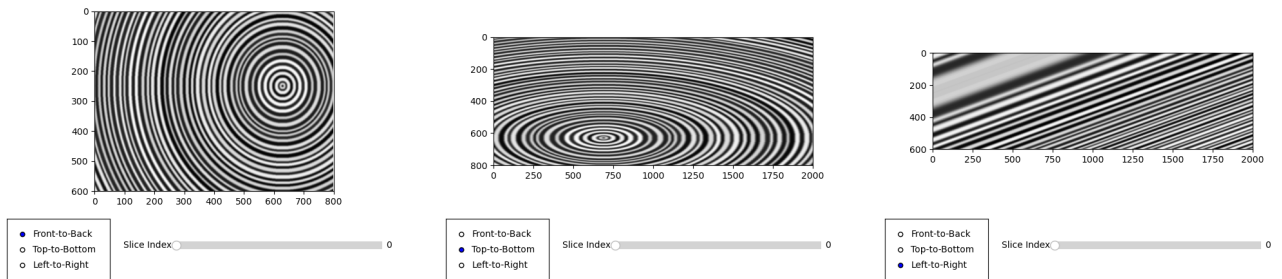


Fig. 11. Phantom for a wooden block of which the rings have an angle of 20 degrees in the height axis.

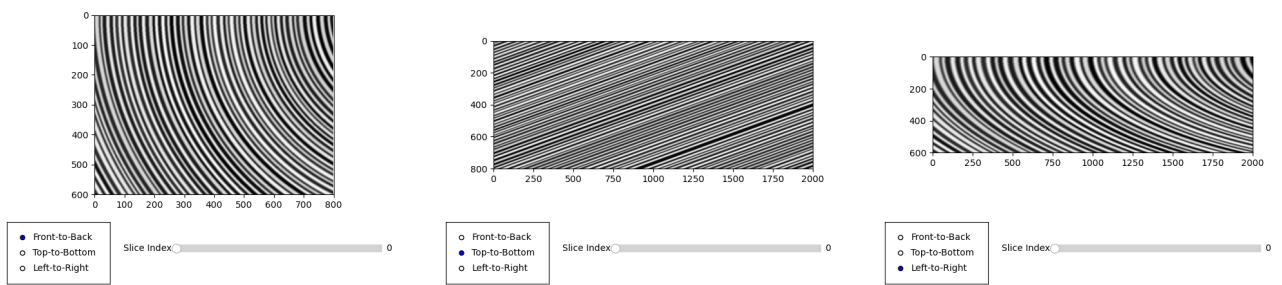
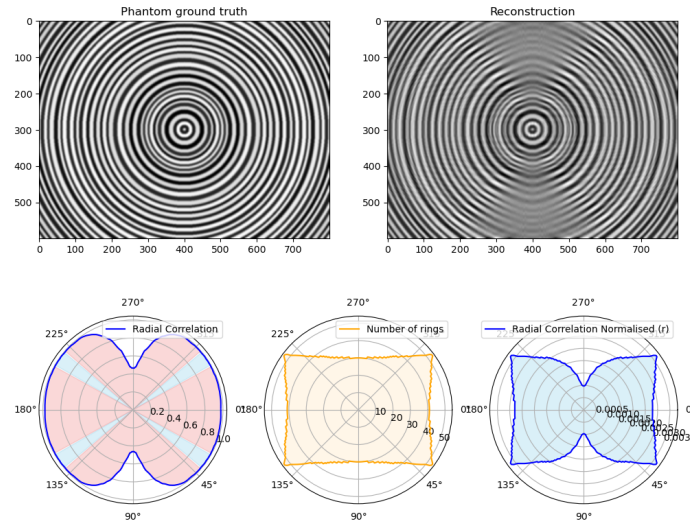


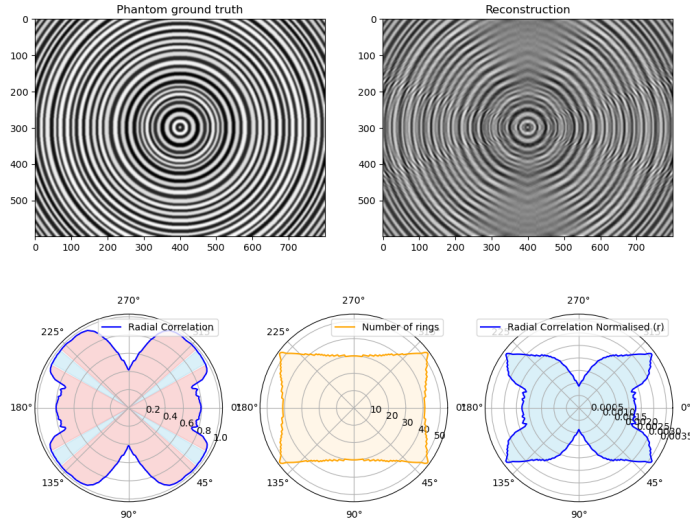
Fig. 12. Phantom for a wooden block of which the rings have an angle of 20 degrees in the width axis.

APPENDIX B RADIAL CORRELATION CALCULATION

This section shows an example of how the WRCOAA and WRCOLA measures are calculated. Figure 13 shows the ground truth of a phantom and its reconstruction. The radial correlation shows the similarity between the reconstruction and the ground truth for each of the 360° , starting from the pith. The number of rings indicates the amount of rings counted in that angle. The Radial Correlation Normalized combines these two measures. Adding the values for each angle results in the WRCOAA score. The WRCOLA score is constructed only from the 20 percent of angles that have the highest ring counts, as is indicated in the blue sections of the bottom left correlation figure.



(a) Example of measurement calculation and reconstruction using cone angle $\beta = 9^\circ$



(b) Example of measurement calculation and reconstruction using cone angle $\beta = 15^\circ$

Fig. 13. Examples of ground truth and reconstruction of phantoms with different cone angles. Below, the radial graphs represent the steps of calculating the WRCOAA and WRCOLA scores, for each of the angles with the pith as the source. Bottom left: correlation, Middle: Ring count, Bottom Right: normalized radial correlation. (a) Shows an example using a cone angle $\beta = 9^\circ$, (b) shows an example using $\beta = 15^\circ$. Example reconstruction at depth slice 9.

APPENDIX C
HORIZONTAL TREE-RING TILT RECONSTRUCTIONS

This section includes Figure 14, containing the reconstructed phantoms, where the tree-ring tilt α is in the horizontal direction. It also includes Figure 15, containing reconstructions where a larger cone angle was used.

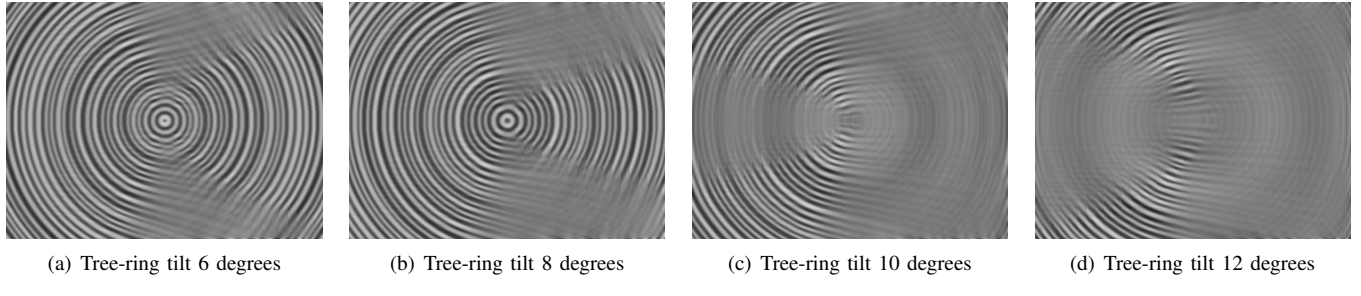


Fig. 14. Reconstructed slices 50 for phantoms with increasing horizontal tree-ring tilt, using cone angle 9 degrees.

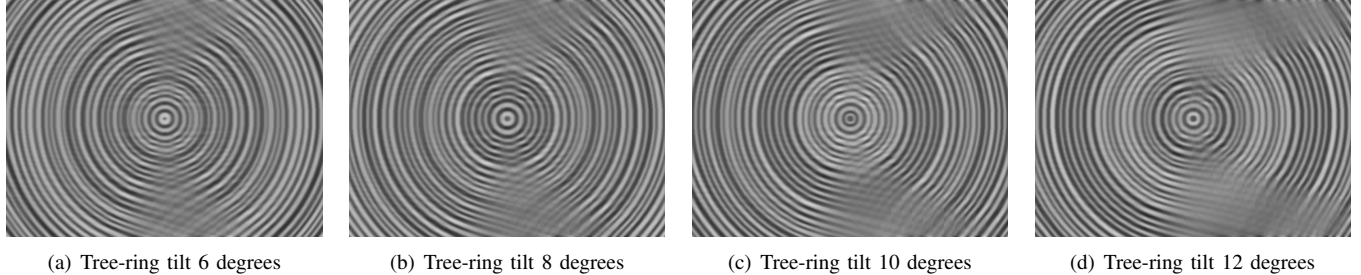


Fig. 15. Reconstructed slices 50 for phantoms with increasing horizontal tree-ring tilt, using cone angle 15 degrees.

APPENDIX D
VERTICAL TREE-RING TILT RECONSTRUCTIONS

This section includes figures of the reconstructed phantoms, where the tree-ring tilt α is in the vertical direction.

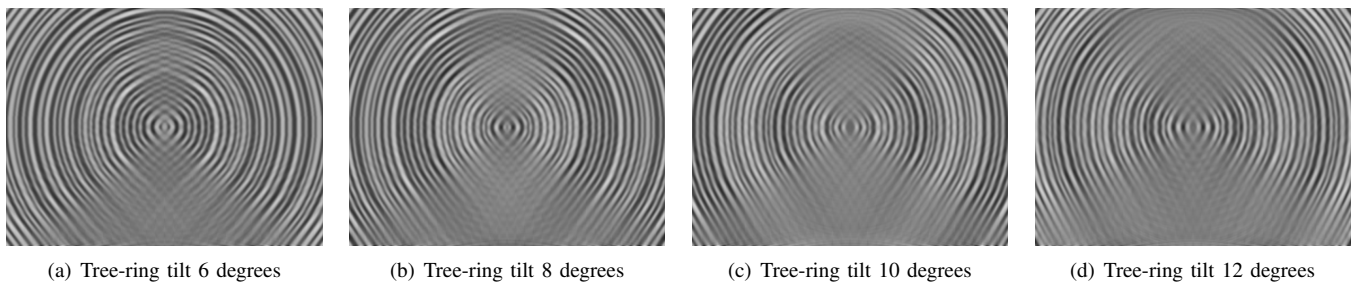


Fig. 16. Reconstructed slices 50 for phantoms with increasing vertical tree-ring tilt, using cone angle 9 degrees.

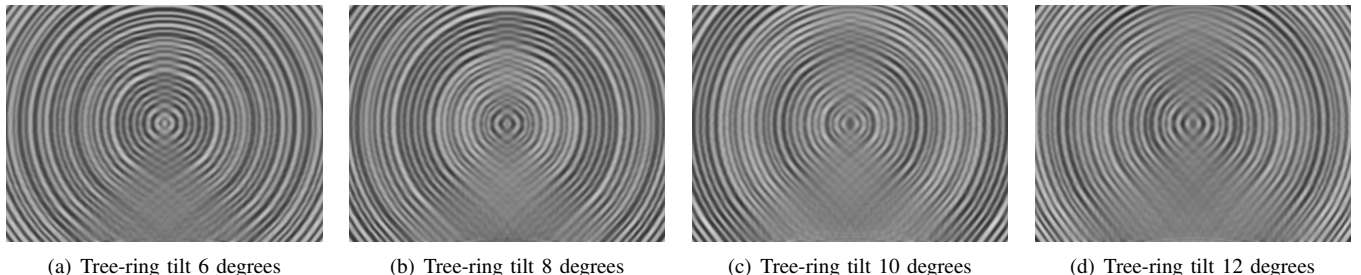


Fig. 17. Reconstructed slices 50 for phantoms with increasing vertical tree-ring tilt, using cone angle 9 degrees.

REFERENCES

- [1] F.G. Bossema *A novel method for dendrochronology of large historical wooden objects using line trajectory X-ray tomography*, <https://doi.org/10.1038/s41598-021-90135-4>, 2021
- [2] W. Aarle, W. Palenstijn, J. Cant, E. Janssens, F. Bleichrodt, A. Dabrowski, J. De Beenhouwer, K.J. Batenburg, and J. Sijbers *Fast and flexible X-ray tomography using the ASTRA toolbox*, <https://doi.org/10.1364/OE.24.025129>, 2016
- [3] F.G. Bossema, J. Dorscheid, A. Kostenko and S.B. Coban. *A line trajectory X-ray tomography dataset of the Hugo de Groot bookchest*. Zenodo. <https://doi.org/10.5281/zenodo.4533923>, 2021
- [4] A. Douglass. *Crossdating in dendrochronology* J. For. 39(10), 825–831, 1941
- [5] H.C. Fritts Tree rings and climate. (Academic Press, London, 1976).
- [6] Zhou Wang, A. C. Bovik, H. R. Sheikh and E. P. Simoncelli, *Image quality assessment: from error visibility to structural similarity*, in IEEE Transactions on Image Processing, vol. 13, no. 4, pp. 600-612, doi: 10.1109/TIP.2003.819861. <https://ieeexplore.ieee.org/document/1284395>, April 2004
- [7] J. Gregor and T. Benson, *Computational Analysis and Improvement of SIRT*, in IEEE Transactions on Medical Imaging, vol. 27, no. 7, pp. 918-924, July 2008, doi: 10.1109/TMI.2008.923696.
- [8] Baillie, M. and Pilcher, Jonathan. (1973). *A simple cross-dating program for tree-ring research*. Tree-Ring Bull. 38. 35-43.